Crystal structure of human cytomegalovirus IL-10 bound to soluble human IL-10R1

Brandi C. Jones*, Naomi J. Logsdon*, Kristopher Josephson*†, Jennifer Cook*, Peter A. Barry‡, and Mark R. Walter*†§

*Center for Biophysical Sciences and Engineering, †Department of Microbiology, University of Alabama, 1025 18th Street South, Birmingham, AL 35294; and ‡Center for Comparative Medicine, University of California, County Road 98 and Hutchison Drive, Davis, CA 95616

Edited by James A. Wells, Sunesis Pharmaceuticals, Inc., South San Francisco, CA, and approved May 23, 2002 (received for review March 12, 2002)

Human IL-10 (hIL-10) modulates critical immune and inflammatory responses by way of interactions with its high- (IL-10R1) and low-affinity (IL-10R2) cell surface receptors. Human cytomegalovirus exploits the IL-10 signaling pathway by expressing a functional viral IL-10 homolog (cmvIL-10), which shares only 27% sequence identity with hIL-10 yet signals through IL-10R1 and IL-10R2. To define the molecular basis of this virus–host interaction, we determined the 2.7-Å crystal structure of cmvIL-10 bound to the extracellular fragment of IL-10R1 (sIL-10R1). The structure reveals cmvIL-10 forms a disulfide-linked homodimer that binds two sIL-10R1 molecules. Although cmvIL-10 and hIL-10 share similar intertwined topologies and sIL-10R1 binding sites, their respective interdomain angles differ by ~40°. This difference results in a striking re-organization of the IL-10R1s in the putative cell surface complex. Solution binding studies show cmvIL-10 and hIL-10 share essentially identical affinities for sIL-10R1 whereas the Epstein–Barr virus IL-10 homolog (ebvIL-10), whose structure is highly similar to hIL-10, exhibits a ~20-fold reduction in sIL-10R1 affinity. Our results suggest cmvIL-10 and ebvIL-10 have evolved different molecular mechanisms to engage the IL-10 receptors that ultimately enhance the respective ability of their virus to escape immune detection.

Human IL-10 (hIL-10) is a pleiotropic cytokine that inhibits cell-mediated immune responses while enhancing humoral immunity (1). Its primary role is to suppress immune function by blocking the synthesis of proinflammatory cytokines [e.g., IL-1, IL-6, IFN-γ, and tumor necrosis factor-α] in T cells, monocytes, and macrophages and by inhibiting the expression of cell surface molecules involved in antigen presentation and costimulation. In addition to its immunosuppressive properties, IL-10 is also a potent growth and differentiation factor for thymocytes, mast cells, and B cells.

hIL-10 cellular responses depend on interactions with its high- and low-affinity cell surface receptors, IL-10R1 and IL-10R2 (2, 3). The first step in the assembly of the biologically active complex is the high-affinity interaction between hIL-10 and IL-10R1. Structural studies show hIL-10 is a noncovalent intertwined dimer in which the twofold related domains comprise four helices (A–D) from one chain and two helices from the other chain (E and F) (4, 5). The crystal structure of a soluble intermediate complex between hIL-10 and soluble (s)IL-10R1 revealed two sIL-10R1s bind the identical twofold related surfaces of the homodimer to form a 1:2 complex (6). Surfaces on hIL-10 and IL-10R1 in this 1:2 complex are thought to form binding sites for IL-10R2, resulting in a hIL-10/IL-10R1/IL-10R2 complex that is able to induce tyrosine phosphorylation by means of JAK kinases (JAK1 and TYK2) and activation of latent transcription factors (STATs) (7–9).

The genomes of human cytomegalovirus (cmv), Epstein–Barr virus (ebv), and the orf poxvirus (orf) each contain ORFs encoding functional viral IL-10 homologs that bind and signal through the hIL-10 cell surface receptors (10–13). cmvIL-10 is the most divergent viral IL-10 homolog discovered thus far, sharing only 27% amino acid sequence identity with hIL-10 whereas ebvIL-10 and orfIL-10 share 83% and 73% identity with hIL-10, respectively. The proposed functional role of each homolog is to exploit the immunosuppressive properties of hIL-10 to subvert cellular immune responses directed against their respective viruses (14). Although the specific role of cmvIL-10 in immune evasion remains to be determined, the overall defense mechanisms of cmv are remarkable, allowing it to establish a persistent lifelong infection in >50% of the population of the world (15). Although largely benign in healthy individuals, cmv is a leading cause of congenital birth defects and causes major health problems in people with compromised immune systems including transplant patients and those infected by HIV-1 (16).

The evolution of the viral cytokines is thought to have optimized their biological properties to the specific needs of the virus rather than the host. Although these differences have not been reported for cmvIL-10, under this selective pressure ebvIL-10 has eliminated the ability of hIL-10 to stimulate thymocyte and mast cell proliferation (17–19). Because the crystal structure of the free ebvIL-10 ligand is essentially identical to hIL-10, functional differences between the molecules have been attributed to ~1,000-fold lower affinity of ebvIL-10 for IL-10R1 on the cell surface (20–23). To date, cmvIL-10 has been shown to suppress proinflammatory cytokine synthesis and MHC class II expression (24). However, the molecular basis for these functional properties has not been defined.

Here we report the 2.7-Å crystal structure of cmvIL-10 in complex with the extracellular domain of its high-affinity receptor (sIL-10R1). In contrast to hIL-10, cmvIL-10 exists as a cystine-linked intertwined dimer. The twofold related domains of the dimer adopt a 130° interdomain angle, compared with 90° for hIL-10, which changes the orientation of the sIL-10R1s in the 1:2 complex. Although cmvIL-10 and hIL-10 share only 27% sequence identity, cmvIL-10 binds to sIL-10R1 with essentially the same affinity as hIL-10. Thus, although ebvIL-10 functional differences are attributed to differences in receptor binding affinity, reorganization of the receptors may modulate cmvIL-10 activity. Structures of the cmvIL-10/sIL-10R1 and hIL-10/sIL-10R1 complexes allow the first direct comparison of the molecular recognition mechanisms used by a human cytokine and its viral mimic.

Materials and Methods

Protein Expression, Purification, and Characterization. sIL-10R1Q6 was expressed and purified as described (25). cmvIL-10 (Townes strain) was secreted into the culture media from *Drosophila* S2 cells (Invitrogen) and purified by affinity chromatography with sIL-10R1 beads. Matrix-assisted laser desorption ionization–time-of-flight MS and SDS/PAGE were used to obtain molecular weights for reduced, nonreduced, and deglycosylated forms

This paper was submitted directly (Track II) to the PNAS office.

Abbreviations: cmv, human cytomegalovirus; ebv, Epstein–Barr virus; hIL-10, human IL-10; s, soluble.

Data deposition: Atomic coordinates and structure factors have been deposited in the Protein Data Bank, www.rcsb.org (PDB ID code 1LQS).

§To whom reprint requests should be addressed. E-mail: walter@uab.edu.

www.pnas.org/cgi/doi/10.1073/pnas.152147499

of the molecule. PNGaseF (New England Biolabs), endoglycosidaseD (Seikagaku America, Rockville, MD), and *O*-glycosidase (Roche Molecular Biochemicals) were used to characterize cmvIL-10 glycosylation. Complex for crystallization experiments was obtained by mixing sIL-10R1Q6 and cmvIL-10 in a 2:1 molar ratio followed by purification by gel filtration chromatography.

Crystallization and Data Collection. cmvIL-10/sIL-10R1 crystals were grown by vapor diffusion at 25°C in hanging drops consisting of 1 μl of receptor complex (10 mg/ml in 20 mM Tris, pH 8.0) and 1 μl of precipitant solution consisting of 100 mM ADA buffer, pH 6.0, 6% PEG-6000, 0.1 M $MgCl_2$, and 0.75% PEG-400. Before setting up the drops, endoglycosidaseD (0.24 microunits/μg complex) was added to the complex followed by incubation overnight at 25°C. Crystals grew in 2–3 days and reached a maximal size of 0.1 mm × 0.3 mm × 0.05 mm. Crystals were cryocooled in a solution consisting of 100 mM ADA, pH 6.0, 6% PEG-6000, 0.1 M $MgCl_2$, and 25% PEG-400. X-ray diffraction data were collected on a Raxis IV image plate detector mounted on a Rigaku RU200 fitted with osmic mirrors (Molecular Structure, Woodlands, TX). Data were indexed, integrated, and scaled with DENZO and SCALEPACK (HKL Research, Charlottesville, VA) (26).

Structure Determination and Refinement. The structure was determined by molecular replacement with CNS Version 1.0 using sIL-10R1Q6 from the hIL-10/sIL-10R1 complex (PDB ID code 1J7V) as the search probe (6, 27). Crossrotation and translation functions clearly identified the position of one sIL-10R1Q6. However, attempts to find the second receptor or locate the position of cmvIL-10 with either hIL-10 (PDB ID code 17JV) or ebvIL-10 (PDB ID code 1VLK) search models were unsuccessful. Phases calculated from the one properly positioned sIL-10R1Q6 were subjected to solvent leveling/flipping phase improvement methods as implemented in CNS (28). An electron density map calculated with the modified phases revealed density corresponding to a second sIL-10R1Q6 chain. The positions of the two sIL-10R1Q6 chains were rigid body-refined and the phase modification procedure was repeated. The resulting map revealed clear electron density for cmvIL-10. Refinement was carried out in CNS (Version 1.0) with noncrystallographic symmetry (NCS) restraints on sIL-10R1Q6 (Table 1). NCS weighting was determined by monitoring of R_{free} (29). Manual model building was performed with O and CHAIN (30, 31). Superpositions, buried surface, and contact distances were obtained with LSQKAB, AREAIMOL, and CONTACT from the CCP4 program suite (32). Model geometry was monitored with PROCHECK (33). Figures were made with the RIBBONS program suite (34).

Solution Affinity Measurements. sIL-10R1 was inactivated after coupling to CM-5 chips for interaction studies. To avoid complexities in interpreting binding data from three different IL-10 molecules nonspecifically coupled to the dextran matrix, apparent equilibrium affinities of cmvIL-10, hIL-10, and ebvIL-10 for sIL-10R1 were obtained by solution affinity with a Biacore 2000. Solutions of each ligand (seven concentrations from 1 to 100 nM for hIL-10 and cmvIL10; nine concentrations from 1 nM to 1 μM for ebvIL-10) were incubated with 10 nM sIL-10R1 and allowed to reach equilibrium at room temperature. Free sIL-10R1 concentrations in each solution were measured on Biacore CM-5 chips immobilized with either ~4,100 or ~1,260 response units of a monomeric IL-10 (35). The mutant IL-10 was coupled by way of a free cysteine, introduced at residue Asn-97, with a 2-(2-pyridinyldithio)ethaneamine (PDEA) linker as described (36). Free receptor concentrations were determined from calibration curves generated before and after measuring the response of solutions with known amounts of sIL-10R1. The errors in sIL-10R1 concentration standards derived from the beginning and end calibration curves were less than 10%. Unknown sIL-10R1 measurements were performed in duplicate and run in random order on each chip. Apparent equilibrium disassociation constants were derived by converting free sIL-10R1 concentrations to fraction sIL-10R1 bound and fitting the data to a 1:1 binding model with ORIGIN 5.0.

Table 1. Data collection and refinement statistics

Data collection	
Resolution (Å)	50–2.7
No. observations	65,855
No. unique	26,564
Redundancy*	2.8 (2.4)
% Complete	92.5 (73.7)
R_{sym}†	0.056 (0.195)
No. of reflections R_{work} (R_{free})	24,727 (1,322)
R_{work}‡ (R_{free})	24.2 (29.5)
rmsd§ bonds (Å)	0.007
rmsd angles (°)	1.35
Overall avg. B-factor (Å²)	52.3
rmsd¶ B (main chain, Å²)	2.8
smsd¶ B (side chain, Å²)	3.7
No. protein atoms	5,627
No. of NAG molecules	2
No. water molecules	48
Ramachandran plot quality	
Most favored (%)	83.2
Additionally favored (%)	15.8
Generously allowed (%)	1.0
Disallowed (%)	0.0

NAG, *N*-acetylglucosamine.

*Parentheses denote statistics in the highest resolution shell of 2.8–2.7 Å.

†$R_{sym} = (\Sigma|I(i) - \langle I(h)\rangle|)/(\Sigma I(i))$ where $I(i)$ is the ith observation of the intensity of a reflection with indices h, k, l and $\langle I(h)\rangle$ is the average intensity of all symmetry equivalent measurements of that reflection.

‡$R_{work} = \Sigma|F_{obs}(h) - F_{calc}(h)|/\Sigma|F_{obs}(h)|$ where $F_{obs}(h)$ and $F_{calc}(h)$ are the observed and calculated structure factor amplitudes, respectively. R_{free} is calculated as R_{work} but for 5% of the data excluded from refinement.

§rms deviations (rmsd) in bond lengths and angles are the deviations from ideal values.

¶rmsd for bonded atoms.

Results and Discussion

Structure Determination. An expression construct containing the full-length cmvIL-10 sequence shown in Fig. 1 was expressed in insect cells and purified by affinity chromatography. cmvIL-10 was incubated with sIL-10R1Q6 (residues 1–214), and the resulting complex was purified by size exclusion chromatography for crystallization trials. cmvIL-10/sIL-10R1Q6 crystals belong to space group C2 (a = 114.29 Å, b = 104.68 Å, c = 91.89 Å, β = 106.49°) and contain one cmvIL-10 dimer and two sIL-10R1Q6s in the asymmetric unit. The structure was solved by molecular replacement and refined with noncrystallographic symmetry restraints to R_{cryst} = 24.2% and R_{free} = 29.5% for all data to 2.7 Å (Table 1.). Amino acids in the cmvIL-10 sequence are numbered based on their correspondence with hIL-10 residues as determined by structure superposition (37). The final model contains cmvIL-10 residues 8–157 for both chains, residues 2–207 and 2–208 for sIL-10R1Q6 chains, 2 *N*-acetylglucosamine residues, and 48 water molecules.

Structure of cmvIL-10. cmvIL-10 bound to sIL-10R1 shares the same intertwined dimer topology observed in hIL-10 (Fig. 1). In contrast to the six helices that form the hIL-10 domain, each domain of cmvIL-10 consists of five α-helices of which helices A,

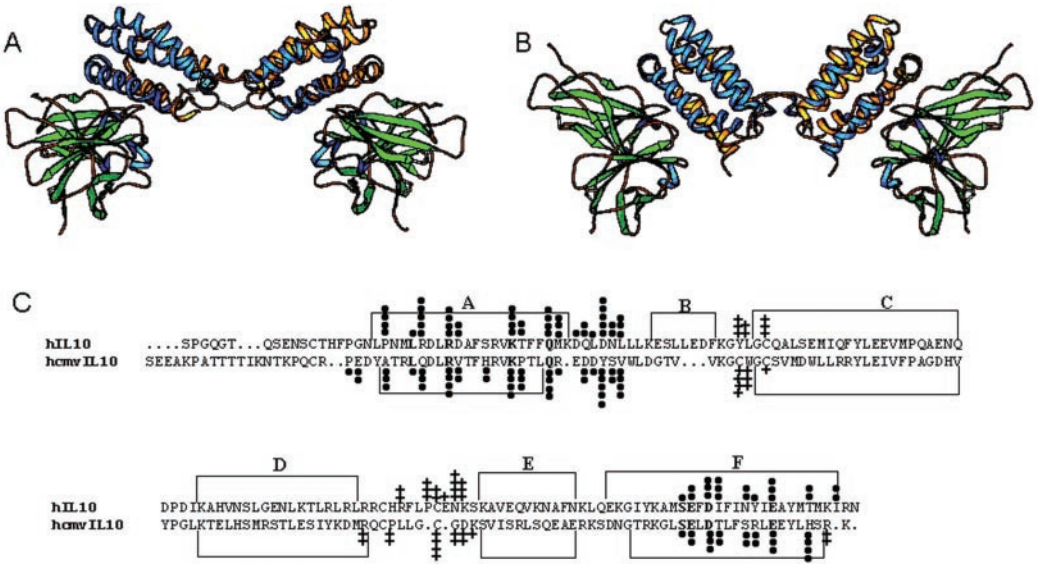

Fig. 1. Structure and sequence of the cmvIL-10/sIL-10R1 complex. (*A*) Ribbon diagram of the 1:2 cmvIL-10/sIL-10R1 complex viewed perpendicular to the twofold axis of cmvIL-10. (*B*) Ribbon diagram of 1:2 hIL-10/sIL-10R1 complex in the same orientation as *A*. (*C*) Structure-based sequence alignment of hIL-10 and cmvIL-10. α-Helices are defined by brackets and labeled. cmvIL-10 or hIL-10 residues that bury surface into sIL-10R1 or into their respective dimer interfaces are marked with circles and crosses, respectively. The amount of buried surface area is denoted by different numbers of circles or crosses with $1 > 5$ Å^2, $2 > 10$ Å$^2 <$ 35 Å^2, $3 > 35$ Å$^2 < 60$ Å^2, $4 > 60$ Å$^2 < 85$ Å^2, and $5 > 85$ Å^2.

C, and D are donated from one peptide chain and helices E and F are donated from the twofold related chain. The sixth helix (helix B) found in hIL-10 is replaced by two consecutive β-turns in cmvIL-10 as a result of to a three-residue deletion in the cmvIL-10 sequence (hIL-10 residues 53–55). Other large structure differences between cmvIL-10 and hIL-10 occur in the N termini of the molecules before helix A, the DE loop that forms most of the dimer interface, and the EF loop that contains an N-linked glycosylation site in cmvIL-10. Despite these differences, cmvIL-10 has successfully mimicked the hIL-10 α-helical scaffold (rms deviation 1.9 Å for 132 Cα pairs) required for presentation of the high-affinity sIL-10R1 binding site.

cmvIL-10 mimics the individual α-helical domains of hIL-10 but not its quaternary structure. The twofold related domains of cmvIL-10 adopt an angle of ~130° with respect to one another compared with the ~90° interdomain angles observed for human and ebvIL-10s (Fig. 1). Despite this difference, cmvIL-10 and hIL-10 each bury 700 Å^2 of surface area into their respective domain interfaces. SDS/PAGE and matrix-assisted laser desorption ionization–time-of-flight MS analysis reveal that the two cmvIL-10 peptide chains in the dimer are linked by an interchain disulfide bond (data not shown). Structural characterization of the domain interface shows Cys-59, located before helix C, forms a disulfide bond with Cys-59′ in the twofold related peptide chain. Because the noncovalent hIL-10 dimer has been shown to dissociate at low protein concentrations, the interchain disulfide bond may increase the stability of the cmvIL-10 dimer and possibly enhance its biological half life (38). The extensive contacts in each interface ensure that the domain angles exhibited by cmvIL-10 and hIL-10 are essentially fixed. Thus, cmvIL-10 has evolved a unique dimer interface and interdomain orientation that is not accessible to hIL-10 or ebvIL-10.

Structure of IL-10R1. sIL-10R1 bound to cmvIL-10 is comprised of two fibronectin type III domains oriented at ~90° to one another (6). As observed in the hIL-10/sIL-10R1 complex, the interface between the N- (D1) and C-terminal (D2) domains of sIL-10R1 display five cytokine binding loops (L2-L6) for interaction with cmvIL-10. Comparison of sIL-10R1s bound to cmvIL-10 and hIL-10 reveals essentially no differences in the backbone conformations of the L2-L6 binding loops or the 90° D1/D2 interdomain angle. (Fig. 2*A*, rms deviation of 0.7 Å for Cαs 4–206). Thus, sIL-10R1 is essentially a rigid molecule that does not reorganize its structure after binding to the human or viral IL-10 ligands.

1:2 cmvIL-10/sIL-10R1 Complex. The cmvIL-10 dimer binds two sIL-10R1s to form a 1:2 cmvIL-10/sIL-10R1 complex. The sIL-10R1 contact surface as well as the orientation of sIL-10R1 on each domain of cmvIL-10 is highly conserved with the hIL-10 bound to sIL-10R1 (Fig. 2*A*, rms deviation 1.4 Å, 336 Cα pairs). However, as a result of the 130° domain angle, sIL-10R1s bound

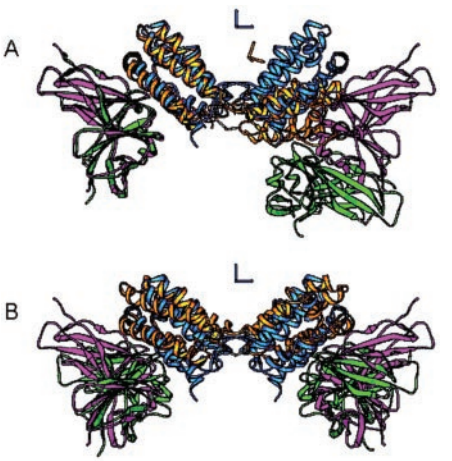

Fig. 2. Superposition of cmvIL-10 and hIL-10 1:2 receptor complexes. (*A*) Superposition of sIL-10R1 bound to cmvIL-10 (green) and hIL-10 (magenta). cmvIL-10 and hIL-10 are colored yellow and blue, respectively. Axes, in the same color as their respective cytokines, are shown representing the location of the twofold axes of cmvIL-10 and hIL-10 dimers. (*B*) Superposition of cmvIL-10 and hIL-10 1:2 complexes by way of the twofold axes of the cmvIL-10 and hIL-10 dimers. Color scheme is as in *A*.

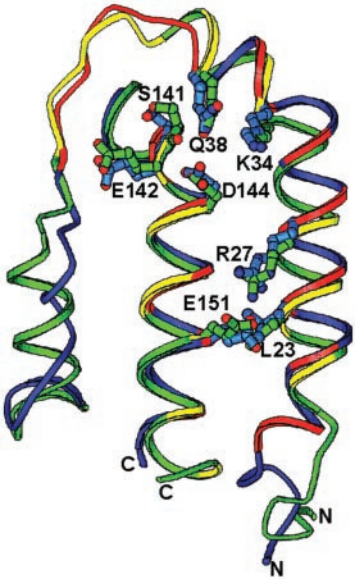

Fig. 3. The sIL-10R1 binding epitope. cmvIL-10 and hIL-10 scaffold residues (10–62 and 137–157 for cmvIL-10, 11–62 and 137–160 for hIL-10) are shown in green and blue, respectively. cmvIL-10 residues that bury surface area into sIL-10R1 are shown in red whereas hIL-10 residues are yellow. Side chains are shown for conserved side chain residues that bury surface area into each interface.

to cmvIL-10 in the 1:2 complex move 25°, relative to the hIL-10/sIL-10R1 complex, toward the putative position of the cell membrane. Despite these differences, the C-terminal ends of the twofold related receptors bound to cmvIL-10 and hIL-10 are separated by 105 and 110 Å, respectively, at the point where they enter the cell membrane. Optimal superposition of the C termini of the receptors (Leu-206 in each complex differ by 5 Å) is obtained by aligning the twofold axes of the CMV and human IL-10 dimers (Fig. 2*B*). Interestingly, the twofold axes are not collinear, suggesting that cmvIL-10 has repositioned its twofold axis to maintain the ~100 Å spacing and the twofold relationship of the receptors. Conservation of these parameters emphasizes their potential importance for optimal IL-10 signal transduction.

The cmvIL-10/sIL-10R1 Interface. cmvIL-10 uses essentially the same structural epitope as hIL-10, comprised of helix A, the AB loop, and helix F, to contact the conserved sIL-10R1 binding loops (L2-L6) in the site I interface (Figs. 1*C* and 3). A total of 25 cmvIL-10 and 21 sIL-10R1 residues bury 945 and 1,007 Å^2 of surface area into the interface, respectively. The sizes of the epitopes are similar to the hIL-10/sIL-10R1 interface, which consists of 24 hIL-10 and 23 sIL-10R1 residues that bury 969 and 1, 132 Å of surface area, respectively. As a result of sequence and structural differences between cmvIL-10 and hIL-10, Pro-16 (6 Å^2), Glu-17 (20 Å^2), and His-31 (27 Å^2) bury surface area only in the cmvIL-10/sIL-10R1 interface whereas Asp-41 (6 Å^2) and Ile-158 (32 Å^2) bury surface area only in the hIL-10/sIL-10R1 complex. The remaining 22 residues form a structurally conserved epitope (rms deviation 1.4 Å for 22 Cα pairs) that despite limited sequence identity bury similar amounts of surface area at each residue position. Contacts are mostly between polar and charged residues that cluster into two distinct interaction surfaces, sites Ia and Ib. Site Ia is located at the intersection of helix F and the AB loop whereas site Ib is located near the N terminus of helix A. The sIL-10R1 binding loops L2-L4 located in D1 interact with site Ia whereas sIL-10R1 D2 loops L5 and L6 interact with site Ib.

cmvIL-10 makes 14 specific hydrogen bond and/or salt bridge interactions with sIL-10R1 in the site I interface (Table 2). All but two of these interactions are also made in the hIL-10/sIL-10R1 site I interface, which consists of 20 contacts. Unique hydrogen bonds in the cmvIL-10/sIL-10R1 complex occur between cmvIL-10 Arg-149 (Tyr-149 in hIL-10) and sIL-10R1 Asn-73 and between cmvIL-10 Thr-145 (Ile-145 in hIL-10) and Arg-96. Almost all of the remaining contacts in the cmvIL-10/sIL-10R1 interface depend on 6 residues that are conserved in the sequences of hIL-10 and all viral IL-10 molecules that bind sIL-10R1. The residues cluster into two groups at the center of site Ia (Lys-34, Gln-38, Ser-141, and Asp-144) and site Ib (Arg-27 and Glu-151) where they make extensive interactions with sIL-10R1 residues Arg-76, Arg-96, and Glu-101 in site Ia and Ser-190 and Arg-191 in site Ib.

Many of the conserved interactions found in both the cmvIL-10/sIL-10R1 and hIL-10/sIL-10R1 complexes involve backbone oxygen and nitrogen atoms that highly depend on the conserved tertiary structures of the binding epitopes (Figs. 3 and 4). The most extreme example is the side chain-independent interaction that occurs between the carbonyl oxygens of the AB loop residues Tyr-44 in cmvIL-10 and Asp-44 in hIL-10 with the main chain nitrogens of Gly-44 on the L2 loop in sIL-10R1. Other interactions make use of side chain atoms, such as Oε1 of Gln-38, which hydrogen bonds to the backbone nitrogen of sIL-10R1 Arg-96. Similarly, the NH1 and NH2 atoms of sIL-10R1 Arg-76 hydrogen bond to the carbonyl oxygen of Gln-38. sIL-10R1 Arg-96 makes extensive interactions with Oδ1 and Oδ2 of Asp-144 but the NH2 atom also hydrogen bonds to the carbonyl

Table 2. Specific contacts in the cmvIL-10 and hIL-10/sIL-10R1 interfaces

sIL-10R1			cmv/hIL-10	R	S	hIL-10
Tyr-43	OH	Oδ1	Asp/Gln-42	3.1	—	—
	OH	O	Ser/Asn-45	—	—	3.3
	OH	Nζ	Lys-138	—	—	3.0
	OH	Oε2	Glu-142	—	—	2.8
Gly-44	**N**	**O**	**Tyr/Asp-44**	**2.8**	**2.9**	**2.7**
Asn-73	Oδ1	NH2	Arg/Tyr-149	2.8	2.9	—
Arg-76	**NH1**	**O**	**Gln-38**	**3.3**	**2.7**	**3.5**
	NH2	**O**	**Gln-38**	**3.2**	**2.7**	**2.7**
	NH1	Oε1	Asp/Gln-42	—	—	3.2
	N$\underline{\varepsilon}$	Oδ1	Tyr/Asp-44	—	—	2.9
	NH2	Oδ1	Tyr/Asp-44	—	—	2.6
	NH2	Oδ2	Tyr/Asp-44	—	—	3.3
Arg-96	**N**	**Oε1**	**Gln-38**	**2.8**	**2.8**	**2.5**
	NH2	**O**	**Ser-141**	**3.2**	**3.4**	**2.9**
	NH2	**Oδ1**	**Asp-144**	**3.2**	**2.8**	**2.5**
	Nε	Oδ2	Asp-144	2.7	2.6	—
	NH2	Oδ2	Asp-144	—	—	2.5
	NH2	Oγ1	Thr/Ile-145	3.4	3.5	—
Glu-101	**Oε1**	**Nζ**	**Lys-34**	**2.7**	**3.2**	**3.7**
Ser-190	O	NH1	Arg-27	3.3	3.0	—
	O	Nε	Arg-27	—	—	3.0
	Oγ	Oε1	Glu-151	3.6	3.0	—
	Oγ	**Oε2**	**Glu-151**	**3.3**	**3.0**	**3.1**
Arg-191	O	Nε2	Gln/Arg-24	2.6	2.8	—
	O	Nε	Gln/Arg-24	—	—	3.1
	NH1	Oε1	Glu-151	—	—	3.3
	NH1	Oε2	Glu-151	—	—	3.0

Contacts are reported if a distance ≤3.4 Å is found in either noncrystallographic symmetry (NCS) related (R and S) cmvIL-10/sIL-10R1 interface or the hIL-10/sIL-10R1 interface (hIL-10). Identical contacts are bolded. cmvIL-10 and hIL-10 residue differences are denoted by cmvIL-10 residue/hIL-10 residue. cmvIL-10 Asp-42 is found in a different conformation in each NCS-related cmvIL-10/sIL-10R1 interface. Its conformation in the S interface, where there is no contact, is very similar to hIL-10 Gln42 in the hIL-10/sIL-10R1 complex.

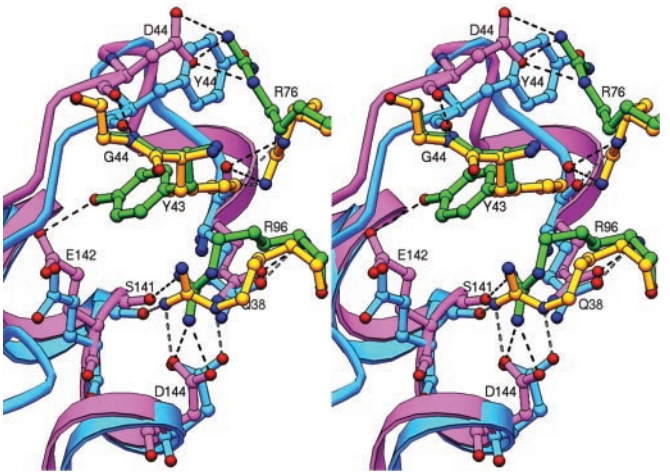

Fig. 4. Stereoview of conformational changes in cmvIL-10 and hIL-10 Site Ia interfaces. cmvIL-10 and hIL-10 residues are shown in cyan and magenta, respectively. sIL-10R1 residues Tyr-43, Arg-76, and Arg-96 are colored yellow in the cmvIL-10/sIL-10R1 complex and green in the hIL-10/sIL-10R1 complex. The second conformation of sIL-10R1 Arg-76 in the hIL-10/sIL-10R1 is not shown for clarity but adopts the same conformation as sIL-10R1 Arg-76 bound to cmvIL-10 (yellow).

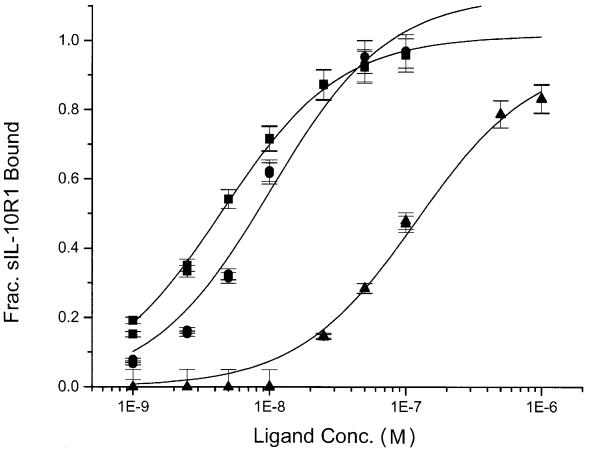

Fig. 5. sIL-10R1 binding properties of the IL-10 homologs. Fraction of bound sIL-10R1 is plotted against increasing concentrations of cmvIL-10 (■), hIL-10 (●), and ebvIL-10 (▲) ($\log_{10}$ scale). Lines are nonlinear fits of the data to a 1:1 binding model.

oxygen of Ser-141 located in the bend in helix F. In site Ib, the carbonyl oxygens of sIL-10R1 Ser-190 and Arg-191 hydrogen bond to the side chain nitrogen atoms of Arg-27 and Gln-24 (Arg 24 in hIL-10), respectively.

Of the 19 sIL-10R1 residues that bury surface area into both cmvIL-10 and hIL-10 site I interfaces, only 3 critical residues (Tyr-43, 110 Å^2; Arg-76, 75 Å^2; and Arg-96, 107 Å^2) located in the center of the binding epitope adopt different side chain conformations in the two complexes (Fig. 4). Surprisingly, sIL-10R1 Tyr-43, which forms extensive interactions with hIL-10 residues Asn-45, Lys-138, and Glu-142, is rotated out of its binding pocket in the cmvIL-10/sIL-10R1 complex. Rotation of Tyr-43 ($\Delta\chi 1 = \sim 110°$) occurs because access to the equivalent binding pocket on cmvIL-10 is sterically prevented as a result of subtle ~1 Å conformational changes in the position of the AB loop relative to helix F. The new position of Tyr-43 interferes (Tyr-43 Cε1-Arg-96 Cδ distance = 2.9 Å) with the side chain conformation of sIL-10R1 Arg-96 in the hIL-10/sIL-10R1 complex. As a result, Arg-96 adopts a new conformation in the cmvIL-10/sIL-10R1 complex that slightly changes its hydrogen bonding pattern with cmvIL-10 Asp-144. sIL-10R1 Arg-76 adopts two conformations in the hIL-10/sIL-10R1 complex. In one conformation (conformation 1) it forms an ion pair with hIL-10 Asp-44 and a hydrogen bond with hIL-10 Gln-42. In its second conformation (conformation 2), the side chain nitrogen atoms hydrogen bond to the main chain oxygen of hIL-10 Gln-38. hIL-10 Asp-44 is replaced by a tyrosine in cmvIL-10, which sterically prevents sIL-10R1 Arg-76 from adopting conformation 1 in the cmvIL-10/sIL-10R1 interface. These conformational changes markedly illustrate how subtle sequence or conformational changes in the AB loop of cmvIL-10 can be transmitted throughout the cmvIL-10/sIL-10R1 interface.

We proposed a putative energetic hotspot for the hIL-10/sIL-10R1 interaction based on sequence conservation of 9 residues among the hIL-10 and several viral homologs that bind to sIL-10R1 (6, 39). The cmvIL-10/sIL-10R1 complex allows us to derive the hotspot from structurally conserved interactions in the cmvIL-10 and hIL-10/sL-10R1 interfaces. It consists of 11 contacts made by 8 IL-10 residues (Gln-24/Arg-24, Arg-27, Lys-34, Gln-38, Asp-44/Tyr-44, Ser-141, Asp-144, and Glu-151) and six sIL-10R1 residues (Gly-44, Arg-76, Arg-96, Glu-101, Ser-190, and Arg-191). These residues bury the same amount of surface area (IL-10 = 530 Å^2 and sIL-10R1 = 350 Å^2) in each complex. With the exception of residue positions 24 and 44, each side chain residue in the hotspot is conserved between cmvIL-10 and hIL-10. Interestingly, residues in the sIL-10R1 binding hotspot are positioned adjacent to one another on helices A and F that are donated from twofold related peptide chains (Fig. 3). Prior structure and stability studies have implicated ion pairs Lys-34/Asp-144 in site Ia and Arg-27/Glu-151 in site Ib as critical for stability of the IL-10 dimer (38). Thus, several residues in the sIL-10R1 binding site are strictly conserved because of their dual functionality requiring them to form high-affinity contacts with sIL-10R1 and stabilize the tertiary structure of the IL-10 fold.

sIL-10R1 Binding and Implications for Altered Signal Transduction. Despite fewer specific contacts with sIL-10R1, solution binding studies reveal the affinity of cmvIL-10 for sIL-10R1 (K_d = 4 nM) is slightly higher than hIL-10 (K_d = 8 nM, Fig. 5). cmvIL-10's sIL-10R1 binding properties are markedly different from ebvIL-10, which in the same assay displays a 130 nM dissociation constant for sIL-10R1. These receptor binding studies along with the structures of cmvIL-10 and ebvIL-10 suggest each viral IL-10 has evolved a different mechanism to engage host IL-10 receptors that may lead to modified IL-10 responses. For example, ebvIL-10 has faithfully mimicked the tertiary structure of hIL-10 but displays a significantly decreased affinity for IL-10R1. In contrast, cmvIL-10 binds sIL-10R1 with essentially the same affinity as hIL-10, but has evolved a very different interdomain angle that changes the orientation of the IL-10R1s in the putative cell surface complex. The possibility that this structural change may alter IL-10 biological properties is not without precedent. Structure-function studies with erythropoietin (EPO) and EPO peptide mimics have shown the orientation of the extracellular domain of EPO receptor is tightly coupled to changes in cytoplasmic signaling events (40, 41). It is well documented that ebvIL-10 is unable to stimulate thymocyte or mast cell proliferation whereas hIL-10 can. To date, cmvIL-10 has been reported to be at least as efficient as hIL-10 in suppressing proinflammatory cytokines in peripheral blood mononuclear cell cultures and cell surface MHC class I and II molecules (24). Whether the structural changes observed for cmvIL-10 result in a biological profile that mimics ebvIL-10,

hIL-10, or is different from both will be the effort of future studies.

We thank Lori Coward for MS. This research is supported by National Institutes of Health Grant AI47300 (to M.R.W.).

1. Moore, K. W., de Waal Malefyt, R., Coffman, R. L. & O'Garra, A. (2001) *Annu. Rev. Immunol.* **19,** 683–765.
2. Liu, Y., Wei, S. H.-Y., Ho, A. S.-Y., de Waal Malefyt, R. & Moore, K. W. (1994) *J. Immunol.* **152,** 1821–1929.
3. Kotenko, S. V., Krause, C. D., Izotova, L. S., Pollack, B. P., Wu, W. & Pestka, S. (1997) *EMBO J.* **16,** 5894–5903.
4. Walter, M. R. & Nagabhushan, T. L. (1995) *Biochemistry* **34,** 12118–12125.
5. Zdanov, A., Schalk-Hihi, C., Gustchina, A., Tsang, M., Weatherbee, J. & Wlodawer, A. (1995) *Structure (London)* **3,** 591–601.
6. Josephson, K., Logsdon, N. J. & Walter, M. R. (2001) *Immunity* **14,** 35–46.
7. Finbloom, D. S. & Winestock, K. D. (1995) *J. Immunol.* **155,** 1079–1090.
8. Wehinger, J., Gouilleux, F., Groner, B., Finke, J., Mertelsmann, R. & Weber-Nordt, R. M. (1996) *FEBS Lett.* **394,** 365–370.
9. Riley, J. K., Takeda, K., Akira, S. & Schreiber, R. D. (1999) *J. Biol. Chem.* **274,** 16513–16521.
10. Lockridge, K. M., Zhou, S. S., Kravitz, R. H., Johnson, J. L., Sawai, E. T., Blewett, E. L. & Barry, P. A. (2000) *Virology* **268,** 272–280.
11. Kotenko, S. V., Saccani, S., Izotova, L. S., Mirochnitchenko, O. V. & Pestka, S. (2000) *Proc. Natl. Acad. Sci. USA* **97,** 1695–1700.
12. Moore, K. W., Vieira, P., Fiorention, D. F., Trounstine, M. L., Khan, T. A. & Mosmann, T. R. (1990) *Science* **248,** 1230–1234.
13. Fleming, S. B., McCaughan, C. A., Andrews, A. E., Nash, A. D. & Mercer, A. A. (1997) *J. Virol.* **71,** 4857–4861.
14. Redpath, S., Ghazal, P. & Gascoigne, N. R. (2001) *Trends Microbiol.* **9,** 86–92.
15. Griffiths, P. D. & Emery, V. C. (1997) in *Clinical Virology*, eds. Richman, D. D., Whitley, R. J. & Hayden, F. G. (Churchill Livingstone, Secaucus, NJ), pp. 445–470.
16. Britt, W. J. & Alford, C. A. (1996) in *Fields Virology*, eds. Fields, B. N., Knipe, D. N. & Howley, P. M. (Lippincott–Raven, Philadelphia), pp. 2493–2523.
17. Vieira, P., de Waal-Malefyt, R., Dang, M. N., Johnson, K. E., Kastelein, R., Fiorentino, D. F., deVries, J. E., Roncarolo, M. G., Mosmann, T. R. & Moore, K. W. (1991) *Proc. Natl. Acad. Sci. USA* **88,** 1172–1176.
18. Go, N. F., Castle, B. E., Barrett, R., Kastelein, R., Dang, W., Mosmann, T. R., Moore, K. W. & Howard, M. (1990) *J. Exp. Med.* **172,** 1625–1631.
19. MacNeil, I. A., Suda, T., Moore, K. W., Mosmann, T. R. & Zlotnik, A. (1990) *J. Immunol.* **145,** 4167–4173.
20. Zdanov, A., Schalk-Hihi, C., Menon, S., Moore, K. W. & Wlodawer, A. (1997) *J. Mol. Biol.* **268,** 460–467.
21. Liu, Y., de Waal Malefyt, R., Briere, F., Parham, C., Bridon, J.-M., Banchereau, J, Moore, K. W. & Xu, J. (1997) *J. Immunol.* **158,** 604–613.
22. Ding, Y., Qin, L., Kotenko, S. V., Pestka, S. & Bromberg, J. S. (2000) *J. Exp. Med.* **191,** 213–224.
23. Ding, Y., Qin, L., Zamarin, D., Kotenko, S. V., Pestka, S., Moore, K. W. & Bromberg, J. S. (2001) *J. Immunol.* **167,** 6884–6892.
24. Spencer, J. V., Lockridge, K. M., Barry, P. A., Lin, G., Tsang, M., Penfold, M. E. & Schall, T. J. (2002) *J. Virol.* **76,** 1285–1292.
25. Josephson, K., McPherson, D. T. & Walter, M. R. (2001) *Acta Crystallogr. D* **57,** 1908–1911.
26. Otwinowski, Z. & Minor, W. (1997) in *Methods of Enzymology*, eds. Carter, C. W., Jr., & Sweet, R. M. (Academic, San Diego), Vol. 276, pp. 307–326.
27. Brünger, A. T., Adams, P. D., Clore, G. M., DeLano, W. L., Gros, P., Grosse-Kunstleve, W., Jian, J., Kuszewski, J., Nilges, M., Pannu, N. S., *et al.* (1998) *Acta. Crystallogr. D* **54,** 905–921.
28. Abrahams, J. P. & Leslie, A. G. W. (1996) *Acta Crystallogr. D* **52,** 30–42.
29. Brünger, A. T. (1992) *Nature (London)* **355,** 472–475.
30. Sack, J. S. (1988) *J. Mol. Graph.* **6,** 224–225.
31. Jones, T. A., Zou, J. Y., Cowan, S. W. & Kjeldgaard, M. (1991) *Acta Crystallogr. A* **47,** 110–119.
32. Collaborative Computational Project, No. 4 (1994) *Acta Crystallogr. D* **50,** 760–763.
33. Lakowski, R. J., Macarthur, M. W., Moss, D. S. & Thronton, J. M. (1993) *J. Appl. Crystallogr.* **26,** 283–290.
34. Carson, M. (1997) in *Methods in Enzymology*, eds. Carter, C. W., Jr., & Sweet, R. M. (Academic, San Diego), Vol. 277, 493–505.
35. Josephson, K., DiGiacomo, R., Indelicato, S. R., Iyo, A. H., Nagabhushan, T. L., Parker, M. H. & Walter, M. R. (2000) *J. Biol. Chem.* **275,** 13552–13557.
36. Cunningham, B. C. & Wells, J. A. (1993) *J. Mol. Biol.* **234,** 554–563.
37. Bachar, O., Fischer, D., Nussinov, R. & Wolfson, H. J. (1993) *Protein Eng.* **6,** 279–288.
38. Syto, R., Murgolo, N. J., Braswell, E. H., Mui, P., Huang, E. & Windsor, W. T. (1998) *Biochemistry* **37,** 16943–16951.
39. Clackson, T. & Wells, J. A. (1995) *Science* **267,** 383–386.
40. Syed, R. S., Reid, S. W., Li, C., Cheetham, J. C., Aoki, K. H., Liu, B., Zhan, H., Osslund, T. D., Chirino, A. J., Zhang, J., *et al.* (1998) *Nature (London)* **395,** 511–516.
41. Livnah, O., Johnson, D. L., Stura, E. A., Farrell, F. X., Barbone, F. P., You, Y., Liu, K. D., Goldsmith, M. A., He, W., Krause, C. D., *et al.* (1998) *Nat. Struct. Biol.* **5,** 993–1004.